THE ROLE OF CLIMATE IN THE DEFORMATION OF A FOLD AND THRUST BELT

A Thesis

by

SEAN KRISTIAN STEEN

Submitted to the Office of Graduate Studies of
Texas A&M University
in partial fulfillment of the requirements for the degree of

MASTER OF SCIENCE

December 2011

Major Subject: Geology

The Role of Climate in the Deformation of a Fold and Thrust Belt

THE ROLE OF CLIMATE IN THE DEFORMATION OF A FOLD AND THRUST BELT

A Thesis

by

SEAN KRISTIAN STEEN

Submitted to the Office of Graduate Studies of
Texas A&M University
in partial fulfillment of the requirements for the degree of

MASTER OF SCIENCE

Approved by:

Chair of Committee,	David Wiltschko
Committee Members,	Robert Korty
	Anne Raymond
	John Spang
Head of Department,	Rick Giardino

December 2011

Major Subject: Geology

ABSTRACT

The Role of Climate in the Deformation of a Fold and Thrust Belt.

(December 2011)

Sean Kristian Steen, B.S., Texas A&M University

Chair of Advisory Committee: Dr. David V. Wiltschko

Theory and experiment show that the rate and geographic distribution of erosion control the rate and pattern of deformation in collisional mountain belts. Enhanced erosion reduces the mass of material that must be moved up and over ramps and uplifted in large folds. In order to test this and related ideas in a natural example, we have compared modeled rainfall to measured thrust sheet displacement, geometry, and internal deformation in the Appalachian fold and thrust belt. We use mean annual precipitation from a global climate model (GCM) as a proxy for rate of erosion. Deformation measurements were made on a portfolio of regional cross sections from Alabama to New England. During the Carboniferous Allegheny orogeny, the Southern Appalachians moved from -30 ° to 0° latitude, whereas the Central and Northern Appalachians lay between -15° and 5° latitude. Mean annual precipitation determined from the GENESIS 2 GCM (Grossman, per. comm.) varied from tropical to arid conditions as the collision both moved north and grew in breadth and height. The Southern Appalachians, which experienced more net rainfall than other regions, generally show more displacement, deeper present day exhumation, and shallower ramps

than regions to the north. The vicinity of the Pine Mountain thrust sheet in the Southern Appalachians experienced the most displacement (~1.5X the Central Appalachian average) and bulk shortening (~1.6X the Central Appalachians) and produced the most eroded material (~1.5X the Central Appalachians). The latitude of the Pine Mountain thrust sheet in the Southern Appalachians received ~20% more rainfall than the Central Appalachians. Although the number of regional detachments and lithologies change from Southern to Central and Northern Appalachians, the change in rainfall both regionally at any one time and as the collision progressed may explain part of the change in structural style from south to north.

ACKNOWLEDGEMENTS

I would like to thank my committee chair, Dr. David Wiltschko, and my committee members, Dr. John Spang, Dr. Anne Raymond, and Dr. Rob Korty, for their guidance and support throughout the course of this research. Special thanks are also extended to Dr. Ethan Grossman for providing the global climate models used in this study and for his time and expertise in the field of paleoclimate reconstruction and interpretation. Thanks also go to my friends and colleagues and the department faculty and staff for making my time at Texas A&M University a great experience.

TABLE OF CONTENTS

Page

LIST OF FIGURES

LIST OF TABLES

1. INTRODUCTION

1.1. Previous Work

Thin skinned fold and thrust belts vary widely in displacement, duration and dimensions. Some of the variability is no doubt a function of the rocks making up the margin that is eventually deformed. However, field work, theory and experiment show that climatic factors such as rate of erosion can also control how deformation of fold and thrust belt progresses. For instance, in the active southern Taiwan orogen, Dadson et al. (2003) show that the highest rates of rock exhumation occur in regions with relatively higher present day rainfall, higher storm frequency and lesser bedrock strength (see also Li, 1976; Liu, 1982; Liew et al., 1993; Fuller et al., 2003). Likewise, in the Himalayas, the youngest AFT cooling ages are confined to a 50-70 km wide sector (Thiede et al., 2004) that experiences focused orographically-induced precipitation (Bookhagen et al., 2005). This narrow sector also is characterized by steep longitudinal river profiles (Seeber and Gornitz, 1983), high relief and rapid exhumation (Thiede et al., 2004). Similarly, in the Andes, the change along-strike in orogen width, depth of exhumation, and rock uplift rate have been attributed to the type and intensity of erosional processes (Garner, 1959).

The displacement, duration and dimensions of ancient mountain belts may also reflect the net precipitation at the time of the orogeny. Hoffman and Grotzinger (1993)

This Thesis follows the style of The Journal of Structural Geology.

propose that exhumation rate controls both the structure and nature of flanking basins in two ancient orogens, the Thelon and Wopmay. Formation of the Wopmay and Thelon orogens occurred by collision on the west and east passive margins of a ~500-km-wide Archean slave craton in the Late Pliocene Epoch, at ~ 1.88 and 1.97 Ma, respectively (Hoffman and Grotzinger, 1993). Hoffman and Grotzinger (1993) observe dramatic differences in the distribution and amount of displacement on faults, orogen breadth, and thickness of synorogenic basin sediments between the two orogens. The cause may be climatic. Paleomagnetic and paleopole reconstructions place the Thelon and Wopmay orogenic fronts at paleolatitudes of ~10°-30° oriented primarily north-south, perpendicular to prevailing trade winds (Hoffman and Grotzinger, 1993). The forced ascent of these winds up the windward slopes of the Thelon orogeny would have cooled the air column, leading to saturation and enhanced precipitation. Conversely, the descent over the leeward slopes would have warmed the air and suppressed precipitation over the Wopmay orogen. Hoffman and Grotzinger (1993) further speculate that orogens such as the Thelon orogen that are formed under relatively wet conditions are deeply exhumed, have a narrow thin-skinned fold and thrust belt, and a poorly preserved, overfilled foreland basin (see Table 1). 'Dry' orogens, such as the leeward Wopmay, have a broad thin-skinned fold and thrust belt, and a well-preserved, under-filled foreland basin (St-Onge, 1984; Hoffman et al., 1988; Jackson, 1988; Thompson, 1989).

Table 1. Characteristics of orogens developed with high and low rates of precipitation and consequent erosion from Hoffman and Grotzinger, (1993)

	High Precipitation Rate	**Low Precipitation Rate**
Erosion	Deep	Shallow
Metamorphic Gradient	Steep	Gentle
Footwall Reactivation	Extensive	Restricted
Thin-Skinned Fold-Thrust Belt	Narrow	Broad
Synorogenic Detritus	Compositionally mature	Compositionally immature
Foreland Basin	Poorly preserved Overfilled Fluvial to shallow marine Progradational stacking	Well-preserved Under-filled Submarine fans Aggradational stacking

Observations and speculation on natural examples have recently been tested with analog and numerical models. The goal of most of these models is to explore the role of erosion on the pattern and intensity of faulting (Mugnier et al., 1997; Persson and Sokoutis, 2002; Whipple and Meade, 2002; Roe et al., 2003; Whipple, 2009). For example, Persson et al. (2004) use a simple sandbox model and numerical surface process model (SPM) to simulate the effects of erosion and river channel incision on internal wedge deformation. During the experiments erosion was enhanced on one half of the model orogen and sedimentation on the other. They find that the side undergoing enhanced erosion retains elevation by reverse faulting. The most intense erosion occurs along long-lived faults. These faults rotate and steepen with increasing erosion (Cobbold et al., 1993; Persson et al., 2004). Additionally, the model orogen width is inversely proportional to the amount of erosion. They hypothesize that changes in faulting are controlled by sedimentary load. For example, increased overburden on the hanging wall of back thrusts both restricts their displacement and inhibits the formation of new ones. Instead, in order to accommodate further shortening, new fore thrusts are formed, and the ones that already exist accommodate larger displacement (Cobbold et al., 1993; Merle and Abidi, 1995; Leturmy et al., 2000). By contrast, increased mass above the frontal thrust increases normal and shear stress at failure along the fore thrust. Strain accommodation is therefore achieved by the formation of back thrusts and the expansion of the thrust-fold belt into the hinterland (Persson et al., 2004).

Mugnier et al. (1997) explore the role of erosion and sedimentation in fracture development in a model orogen with two levels of detachment. Specifically, their

models were constructed of four layers, two of which were weak material to simulate detachments. The stacking order from bottom to top was a basal weak layer. 1mm thick, composed of glass microbeads, a competent sand layer (5mm), another weak layer 2 mm thick composed of a Newtonian viscous silicone fluid, capped by an upper competent sand layer 7 mm thick. Both sand layers were composed of the same sand and glass powder to simulate the Mohr-Coulomb-Byerlee behavior of brittle rocks. The upper weak unit simulates an evaporite horizon that is virtually insensitive to the value of mean stress. They find that shortening in the lower sand layer is accommodated by the formation of a duplex. In models without either syntectonic sedimentation or erosion, thrusts and symmetrical folds form in the upper competent layer. With syntectonic sedimentation and no erosion, back-thrusts formed in the initial stages of shortening become inactive before 10% shortening after which structures are formed above the duplex. Anticline spacing is more than double those in experiment 1 and the difference between their geometries is not limited to the presence or absence of synorogenic sediments. Finally, with both syntectonic sedimentation and erosion imposed during deformation, only back thrusts form and then only in the lower sand layer. In addition, numerous reactivations occur in the hinterward part of the duplex.

1.2. Effect of Erosion on Thrust Motion

Erosion during deformation reduces the mass that must be uplifted during deformation if that eroded mass is efficiently transported elsewhere. For individual

structures, the location of uplift is localized above thrust ramps and large folds. The work done against gravity is only one part of the total work that must be done to move a thrust sheet forward. Following Mitra and Boyer (1986),

$$W_t = W_p + W_b + W_i + W_g \quad (1)$$

where W_t is the total work, W_p is the work required for fault propagation, W_b is the work required to overcome friction on the basal fault, W_i is the work consumed by internal deformation of thrust sheets, and W_g is the work done against gravity. W_b is a function of the shear resistance of the basal detachment, fault length and displacement along the basal detachment. W_i is proportional to the thrust sheet thickness and rock strength. Mitra and Boyer (1986) propose that

$$W_g \approx \rho \cdot U \cdot h \cdot g \cdot D, \quad (2)$$

where, ρ is rock density, U is the cross-sectional area of material moved above a datum, h is ramp height, g is acceleration due to gravity, and D is displacement. Based on equations (1) and (2), erosion would effectively decrease the total work required for fault motion by decreasing the total mass that must be moved up and over a ramp. Reduced overburden also decreases the shear resistance of frictional faults.

The purpose of this project is to explore whether there is a change in deformation intensity and character at the scale of individual structures over the length of an orogen as a function of mean annual rainfall. We are using rainfall as a proxy for erosion, as discussed more fully below.

2. THE APPALACHIAN FOLD AND THRUST BELT

We seek a location where, 1) the structures and their evolution are relatively well known, 2) the syn-tectonic mean annual rainfall or some proxy can be measured or reconstructed and, 3) there is considerable variation in rainfall either geographically or over the life of the orogen. The purpose of criterion 3) is to examine changing rainfall over the same or similar rocks through time. The Carboniferous Allegheny orogeny of the Appalachians provides a useful balance among these three requirements.

2.1. Geology

The Appalachian fold and thrust belt has been the subject of geologic investigation since the early nineteenth century (e.g. Rogers and Rogers, 1843; Rogers, 1850; Shaler, 1877; Willis, 1893; Keith, 1895; see summaries by Rodgers, 1970 and Hatcher, 1989). It is approximately 480 km wide and extends over ~2500 km from the southern Gulf Coastal plain of Alabama through the Canadian provinces of Québec and Newfoundland (Fig. 1). The last and most intense event in the formation of the Appalachian chain is the collision between Laurentia and Gondwana, during the Allegheny orogeny (e.g. Rodgers, 1970; Hatcher et al., 1989). Rb-Sr whole rock ages on Alleghanian plutons and $^{40}Ar/^{39}Ar$ cooling ages constrain deformation to between the Middle Mississippian (~330 Ma) and late Guadalupian (~265 Ma) Epochs (e.g. Dallmeyer et al., 1986; Secor et al., 1986).

Figure 1. Simplified tectonic map of eastern North America showing structural divisions and physiographic provinces of the Appalachian fold and thrust belt. A) The Central and Southern Appalachians. B) The Northern Appalachians. PMT, Pine Mountain Thrust. Cross-sections are shown as bold lines; sections labeled 1 to 29 are from Woodward et al. (1985) and references therein. The circled star is the location of Roanoke, Virginia, which marks the division between the Southern and Central Appalachians. The plane star shows the location of New York, NY which marked the division between the Central and Northern Appalachians. Base map and surface structures are modified from Hibbard et al. (2003) Map 2096 A & B. Physiographic provinces are based on descriptions from Hatcher et al. (1989).

Simplified tectonic map of eastern North America showing structural divisions and physiographic provinces of the Appalachian fold and thrust belt.

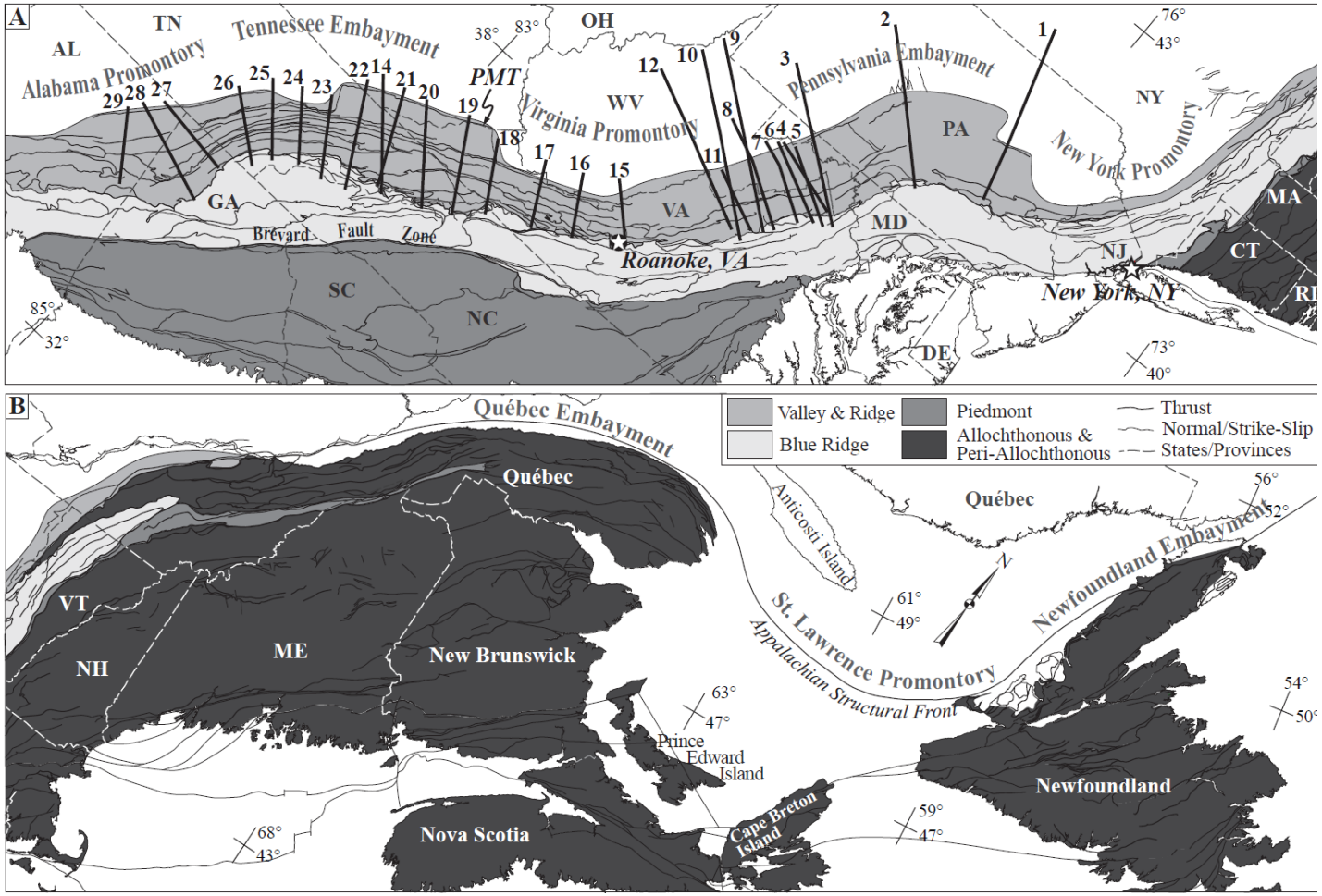
A
AL
TN
Tennessee Embayment
Alabama Promontory
OH
38°
83°
PMT
WV
Virginia Promontory
Pennsylvania Embayment
PA
NY
76°
43°
New York Promontory
GA
Brevard Fault Zone
VA
MD
NJ
Roanoke, VA
New York, NY
MA
CT
RI
SC
NC
85°
32°
DE
73°
40°
B
Québec Embayment
Québec
Valley & Ridge
Blue Ridge
Piedmont
Allochthonous &
Peri-Allochthonous
Thrust
Normal/Strike-Slip
States/Provinces
Anticosti Island
56°
52°
VT
NH
ME
New Brunswick
61°
49°
St. Lawrence Promontory
Appalachian Structural Front
Newfoundland Embayment
63°
47°
Prince
Edward
Island
54°
50°
Newfoundland
68°
43°
Nova Scotia
Cape Breton
Island
59°
47°

The Appalachian orogen can be divided formally along strike into the Southern, Central and Northern regions based on structural style, the extent of synorogenic deposits and the location of promontories and embayments (Fig. 1). The Southern Appalachians extend from the coastal onlap in Alabama to Roanoke, Virginia. In this region the structures are collectively convex toward the craton, forming the Tennessee Embayment (Thomas, 1991). The Central Appalachians extend from Roanoke, Virginia to eastern New York State, a region termed the Pennsylvania Embayment by Thomas (1991). The Central and Southern Appalachians can be further divided across strike into structural provinces on the basis of similar topographic expression, stratigraphy, and structure. From west to east these are the Plateau, Valley and Ridge, Blue Ridge, Piedmont, and Coastal Plain (e.g., Rodgers, 1970; Hatcher, 1989).

The Northern Appalachians extend from eastern New York to the northern Peninsula of Newfoundland. Rocks in the Northern Appalachians primarily consist of accreted terrains which are unrelated to Alleghenian deformation. Unfortunately, the Carboniferous sedimentary record of the Appalachians become very narrow and distributed in isolated basins through much of New England and the Maritime Provinces. It was not possible to obtain measurements of Allegheny structures that could be compared to deformation in the Central and Southern Appalachians. We therefore focus on the Plateau, Valley and Ridge, and Blue Ridge structural provinces of the Southern and Central Appalachians where Alleghenian deformation can be adequately measured.

The Plateau Province of the Southern and Central Appalachians is bound on the east by the more intensely folded and faulted rocks of the Valley and Ridge and to the

west by essentially undeformed cratonic rocks (Fig. 1). South of Roanoke, VA exposed structures are thrust faults and associated ramp anticlines. By contrast, there are few large faults exposed in the Central Appalachians. The most prominent structures are folds with wavelengths of 10's of km and limb dips of a few degrees. The Plateau province is either narrow or not a useful division in the Northern Appalachians.

The Southern Appalachian Plateau includes two relatively competent lithotectonic units (Fig. 2). The lowermost one is the upper Cambrian to Ordovician carbonate sequence whereas the upper one is Lower Carboniferous sandstone, siltstones and shales. Beneath each of these are incompetent horizons in which the prominent detachments lie. The two detachment horizons are the sandstone and shale of the Cambrian Rome through Conasauga formations and the Devonian Chattanooga Shale (Fig. 2). In the Central Appalachians, the stratigraphic section of the Plateau includes one relatively competent layer, the Cambro-Ordovician carbonates and one relatively weak layer, the Devonian-Mississippian shales.

The Valley and Ridge province is significantly more deformed than the Plateau. Between Roanoke and New York, Valley and Ridge fold wavelengths are typically half that of the Plateau province but with amplitudes that are an order of magnitude greater. The Plateau-Valley and Ridge boundary is defined as the last outcrop, going west, of Devonian rocks. In Pennsylvania and New York it is called the Allegheny Structural Front and is well-defined through much of the Central region (Price, 1931) but plunges out to the south, near Alabama. The Southern Appalachian Valley and Ridge is characterized by thrust sheets whose traces may extend 100's of km along strike. In

Figure 2: Schematic stratigraphy, lithotectonic units, and deformation mechanisms in the Southern and Central Appalachians. DH, detachment horizon; FSF, flexural slip folding; LPS, layer parallel shortening; VRP, Valley and Ridge province; BPS, bedding parallel slip; Sil. and S, Silurian age rocks; Ord., Ordovician; D, Devonian; Miss and M, Mississippian; P, Pennsylvanian; PC, Precambrian. Modified from Wiltschko and Geiser (1989) in Hatcher et al. (1989).Schematic stratigraphy, lithotectonic units, and deformation mechanisms in the Southern and Central Appalachians

Schematic stratigraphy, lithotectonic units, and deformation mechanisms in the Southern and Central Appalachians

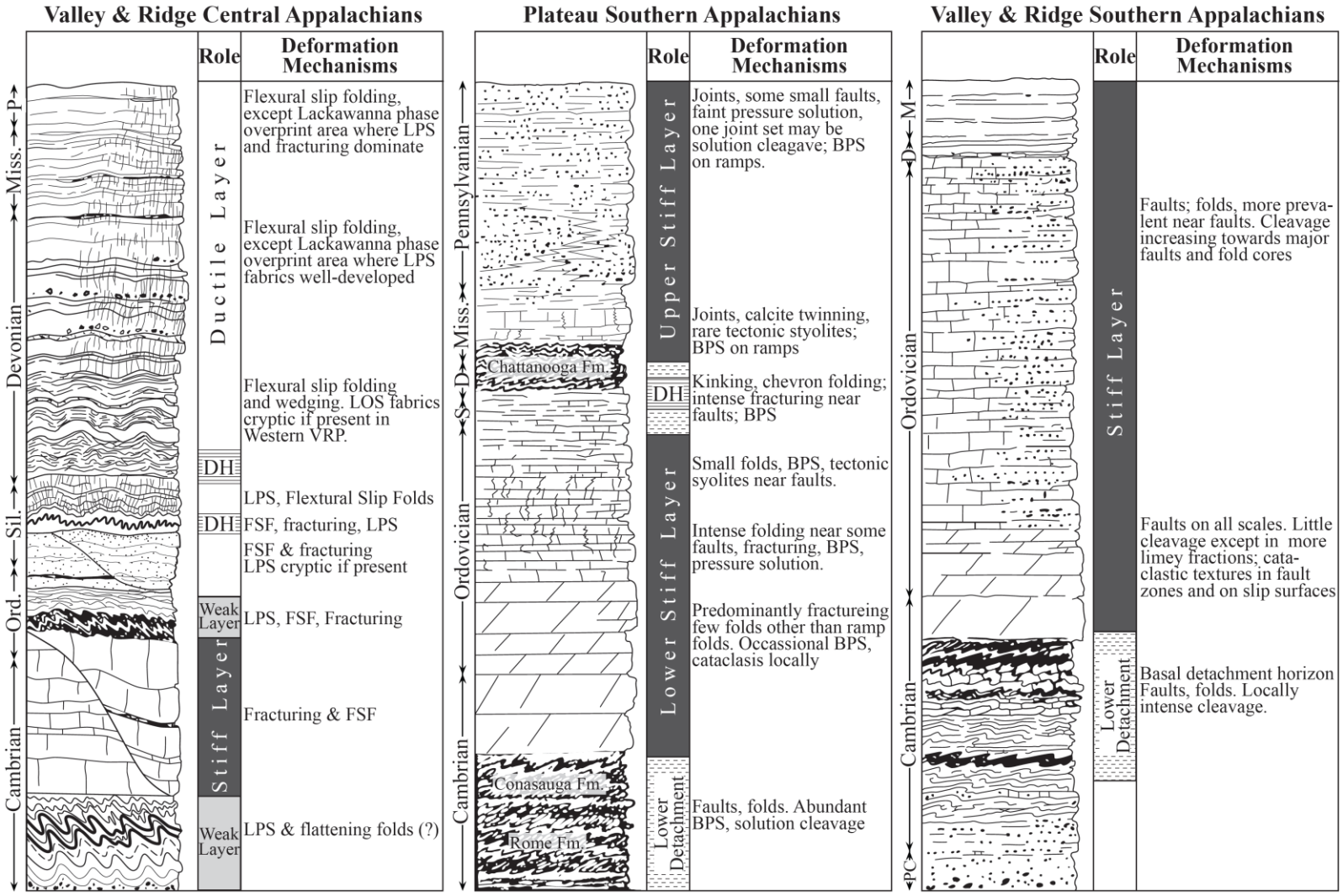
Valley & Ridge Central Appalachians
Role
Deformation Mechanisms
Cambrian
Ord.
Sil.
Devonian
Miss.
P
Ductile Layer
Flexural slip folding, except Lackawanna phase overprint area where LPS and fracturing dominate
Flexural slip folding, except Lackawanna phase overprint area where LPS fabrics well-developed
Flexural slip folding and wedging. LOS fabrics cryptic if present in Western VRP.
DH
LPS, Flextural Slip Folds
DH
FSF, fracturing, LPS
FSF & fracturing
LPS cryptic if present
Weak Layer
LPS, FSF, Fracturing
Stiff Layer
Fracturing & FSF
Weak Layer
LPS & flattening folds (?)
Plateau Southern Appalachians
Role
Deformation Mechanisms
Cambrian
Ordovician
S
D
Miss.
Pennsylvanian
Chattanooga Fm.
Conasauga Fm.
Rome Fm.
Upper Stiff Layer
Joints, some small faults, faint pressure solution, one joint set may be solution cleagave; BPS on ramps.
Joints, calcite twinning, rare tectonic styolites; BPS on ramps
DH
Kinking, chevron folding; intense fracturing near faults; BPS
Lower Stiff Layer
Small folds, BPS, tectonic syolites near faults.
Intense folding near some faults, fracturing, BPS, pressure solution.
Predominantly fractureing few folds other than ramp folds. Occassional BPS, cataclasis locally
Lower Detachment
Faults, folds. Abundant BPS, solution cleavage
Valley & Ridge Southern Appalachians
Role
Deformation Mechanisms
Cambrian
Ordovician
D
M
PC
Stiff Layer
Faults; folds, more prevalent near faults. Cleavage increasing towards major faults and fold cores
Faults on all scales. Little cleavage except in more limey fractions; cataclastic textures in fault zones and on slip surfaces
Lower Detachment
Basal detachment horizon Faults, folds. Locally intense cleavage.

addition, where measurable, the thrust displacement can reach 10's of km.

The Blue Ridge-Valley and Ridge boundary is characterized by the first appearance of Precambrian rocks. The Southern Appalachian Valley and Ridge -Blue Ridge province boundary is generally a large fault or zone of several faults. In the Central Appalachians, exposed thrusts are typically small (only a few kilometers). The Blue Ridge is made up of metamorphosed, multiply deformed rocks. Important lithotectonic units include: 1) the Lower Cambrian quartzite, arkoses and conglomerates that and 2) the Upper Proterozoic basaltic lavas (in VA), graywackes and other clastics atop Precambrian basement.

2.2. Carboniferous Rainfall and Paleogeography

During the Carboniferous Allegheny orogeny the Southern Appalachians lay within 0° and 30° S latitude (e.g., Scotese et al., 1999). In addition, the trend of the orogen at this time was approximately 070° to 080°. By contrast, the Central and Northern Appalachians trend 050° and lay within 15° S and 5° N latitude. These differences in latitude during active deformation suggest that the Central and Northern Appalachians would have experienced different climate conditions than the Southern Appalachians. Moreover, northward drift of the Appalachians as the collision progressed would cause a change in climate through time. We specifically find mean annual rainfall over the time interval of interest from a global circulation model as described below.

3. DATA AND METHODOLOGY

3.1. Measuring Deformation

The source of deformation measurements for the Central and Southern Appalachians is a suite of balanced cross-sections from Woodward (1985). Section lines are generally strike-normal, with an average spacing of less-than 50 km between northern Alabama and New York (Fig. 1). An attempt was made to identify the major structures in each section yet include all deformation. Major thrust sheets are defined on the basis of common detachments, lateral continuity with adjacent sections, and timing. Within the major thrust sheets are imbricates and folds that are translated with the major structure, and in the case of imbricates, do not cut the bounding detachments. The displacement and dimensions of these structures are included with the major structure. We will also note the youngest and oldest stratigraphic units that comprise each sheet. The list of parameters measured on each section is given in Table 2. Measurements were made on both major and subsidiary structures. Major thrust sheets or folds we refer to as first-order. Subsidiary structures we refer to as second-order. We have used the subscript, *i,* on the quantities that we measured to indicate that the measurement was taken on a second order structures (Table 2; Figure 3). For thrust sheet displacement, *d*, we have measured the offset of presumably competent units such as the Cambro-Ordovician carbonates. We use d_i for displacement on second-order features. To

Table 2. Description of variables and measurements used to define deformation along-strike in the Central and Southern Appalachian Fold and Thrust Belt (see Fig. 3).

Summary of Deformation Parameters		
1st Order Measurements	*Calculated*	
d = Thrust sheet displacement	$\mathcal{D} = \Sigma\,(d+d_i)$	Total displacement
ℓ = Thrust sheet length	$T = t + c$	Thickness of displaced material
t = Thrust sheet thickness	$A = T \cdot \ell$	Thrust sheet area
c = Thickness of cover sediments	$E \approx h \cdot d$	Area of eroded rock, 1st order
h = Ramp height	$E_i \approx d_i \cdot h_i$	Area of eroded rock, 2nd order
ϕ = Ramp angle	$\mathcal{E} \approx \Sigma\,(E+E_i)$	Total area of eroded rock, entire cross section
2nd Order Measurements	$L_0 = \Sigma\,\ell$	Undeformed section length
d_i= Thrust sheet displacement		
t_i = Thrust sheet thickness	$L_d = L_0 - \mathcal{D}$	Deformed section length
h_i= Ramp height	$\Delta L = \frac{(L_0 - L_d)}{L_0}$	Bulk shortening of an entire cross section
ϕ_i= Ramp angle		

Definition of measurements made on the cross sections.

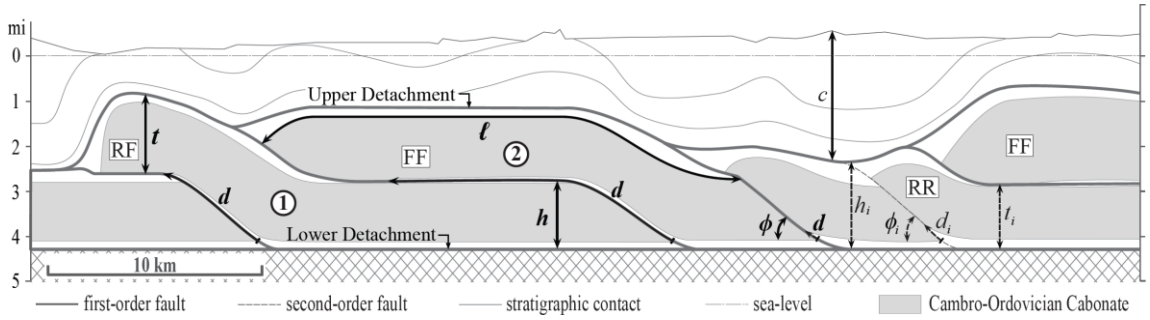

Figure 3: Definition of measurements made on the cross sections. Bold italic text and solid bold lines mark measurements on first-order, structures or those measured at the scale of major thrust sheets. Plain italic text and dashed lines indicate measurements of second-order subsidiary structures. RR, ramp on ramp; RF, ramp on flat and FF, flat on flat. Circled numbers 1 and 2 label thrust sheets discussed in text. See Table 2 for description of variables. Cross-section has been modified from section 3 (see Fig. 2), Shumaker (1972; 1982) in Woodward (1985).

determine the total displacement accumulated on all first and second order faults, $\mathcal{D}$, we have summed the values d and d_i for all thrust sheets in each cross-section.

The length of each thrust sheet, ℓ, is the distance along a competent unit from the rearward footwall cutoff to the frontal hanging wall cutoff. The thickness of first order thrust sheets, t, is defined as the distance from the lower detachment to the upper detachment measured perpendicular to bedding at the thickest part of the thrust sheet. We use t_i for structures found within the larger, first order, structure. Unlike the Southern Appalachians, in the Central Appalachians there are two detachment horizons that separate sections of rock that deformed in different ways. The rocks between the upper and lower detachments deform largely as thrust sheets with typical ramp-flat geometry. Rocks above the upper detachment are better characterized as folds on several scales. In the Central Appalachians we define the thickness of cover, c, as the folded strata above the upper detachment measured perpendicular to bedding (Table 2; see Fig. 3). This thickness is added to the thickness of the underlying thrust sheet, t, to provide a minimum estimate of the original transported rock thickness, T. We determine the thrust sheet area, A, by multiplying the thrust sheet length, ℓ, and the average thrust sheet thickness, T, to examine regional trends in relative thrust sheet size.

The ramp height, h, is the distance measured perpendicular to bedding between the upper and lower detachments connected by a thrust ramp. h and t are often nearly equal, but not always. For example, the thickness, t, of thrust sheet *1* in Figure 3 may appear to equal the ramp height, h, for thrust sheet *2*. However, for thrust sheet *1*, t is measured at the thickest part of that thrust sheet whereas, the ramp height, h, for thrust

sheet *2* can only be measured at the thickest part of thrust sheet *1* that is overlain by the thrust sheet 2. The ramp angle, ϕ, is measured with respect to bedding in the footwall. We use ϕ_i for higher order ramp angles. Not all higher order ramp heights and angles are measurable. In those cases, we record an average of those ramp heights and angles that could be measured.

Assuming ramp-flat thrust geometries, the area of eroded rock resulting from displacement on a single thrust sheet may be approximated by $E \approx d \cdot h$. The additional area of eroded material caused by displacement on internal structures, E_i, is calculated by multiplying the values d_i and h_i. To determine the cumulative area of eroded material, $\mathcal{E}$, we have summed E and E_i for all thrust sheets in each cross-section.

A measure of average shortening of each cross section, ΔL, is:

$$\Delta L \approx \frac{L_0 - L_d}{L_0}\% \tag{5}$$

where L_0 is the sum of the lengths of each thrust sheet and L_d is the deformed section length. L_d, is determined by subtracting the total displacement, $\mathcal{D}$, from the undeformed length, L_0.

Given the present level of exhumation only a minimum estimate of many of the length measurements are possible. For instance, if the hanging wall cutoff is eroded, the values d, d_i, ℓ, t, and t_i can only be measured to the eroded surface and therefore are minima. In addition, in the Southern Appalachians a number of first order thrust ramps are partially eroded. It is not known whether these thrust faults connected upper and basal detachments or the basal detachment and the surface. It is therefore not known whether two levels of detachment existed in much of the Southern Appalachians during

deformation. In these cases, the ramp heights measured to the eroded surface are clearly a minimum.

As a comparative estimate of displacement, we have also noted the relative distance between hanging wall and footwall cutoffs. In order of displacement from most to least (Fig. 3), the three displacement categories are flat-on-flat (FF), ramp-on-flat (RF) and ramp-on-ramp (RR). These categories of thrust sheet geometry refer to the relative position of the center of the hanging wall ramp with respect to the center of the footwall ramp. For example, in a ramp-on-ramp geometry the center of the hanging wall ramp is not displaced further than half the length of the footwall ramp. For a ramp-on-flat structure the center of the hanging wall ramp has been displaced further than half the length of the footwall ramp and sits on the upper footwall flat. For a flat-on-flat geometry displacement is large enough for the lower hanging wall flat to lie on the upper footwall flat. While actual measurements are preferred, these categories provide another relative measure of displacement.

3.2. Climate Model of Mean Annual Precipitation

To understand the evolution of erosion through time we examine mean annual precipitation for the Carboniferous simulated with the GENESIS 2 Global Climate Model. First developed at NCAR (Pollard and Thompson, 1995), GENESIS (Global ENvironmental and Ecological Simulation of Interactive Systems) is widely used for both paleoclimate and future climate application (Bonan et al., 1992; Crowley et al.,

1993; Otto-Bliesner, 1993; Pollard and Schulz, 1994; Wilson et al., 1994; Barron, 1995; Sloan and Rea, 1996; Pollard and Thompson, 1997). GENESIS couples a three-dimensional Atmospheric General Circulation Model (AGCM) to the modeled physical effects of vegetation, soil or land ice, and snow. Sea-surface temperatures and sea-ice are computed using a 50-m slab oceanic layer and a dynamic sea-ice model, respectfully. A Land Surface Transfer Model (LSX) accounts for the near-surface physical effects of vegetation, soil and ground-water on flux parameters of heat and moisture. A six-layer soil model accounts for heat diffusion, water transport, transpiration, and freezing and thawing of soil ice in a vertical column to a depth of 4.25 m (Pollard and Thompson, 1994). Both atmospheric and surface processes are represented on a spherical grid defined by coordinates of latitude, longitude, and height, the latter the being vertical distance from some geoidal reference. AGCM grid resolution is spectral T31 (~3.75° x 3.75°) with 18 levels; LSX grid resolution is 2° x 2° (Pollard and Thompson, 1997).

Global mean annual precipitation is modeled at 20 Ma increments between 280 and 360 Ma (Grossman et al., 2002). The following are model inputs: 1) continental configuration (Scotese et al., 1999), 2) estimated topography (Scotese, in prep.), 3) modern (pre-industrial) 1% per 100 Ma insulation, and 4) atmospheric pCO_2 levels that are 1x and 4x pre-industrial levels (280 and 1120 ppm respectively). The results represent global mean precipitation averaged for the final 10 years (once steady-state conditions are achieved) in a 25-year simulation. The results of each simulation are presented as contoured rainfall quantity in a Universal Transverse Mercator (UTM)

Figure 4: GENESIS 2 GCM: Global Mean Annual Precipitation, 320 Ma. Shaded contour maps of global mean annual precipitation in the Late Mississippian Epoch (~320 Ma). Both (A) and (B) from Grossman et al. (2002) in Universal Transverse Mercator (UTM) projection. (A) Model mean annual precipitation for entire globe. Grey dashed line outlines land mass input to model. Inset box outlines the region shown in (B). (B) Rainfall (shaded contours) over the Appalachian Fold and Thrust Belt (thick black line). Solid grey lines show the approximate outline of the United States, North and South America and Africa. For this model continental configuration and estimated topography are from Scotese et al. (1999) and (Scotese, in prep.), respectively. Also for this model, insulation was set at the modern (pre-industrial) value of 1% per 100 Ma, and atmospheric pCO_2 of ~280 ppm).

GENESIS 2 GCM: Global Mean Annual Precipitation, 320 Ma

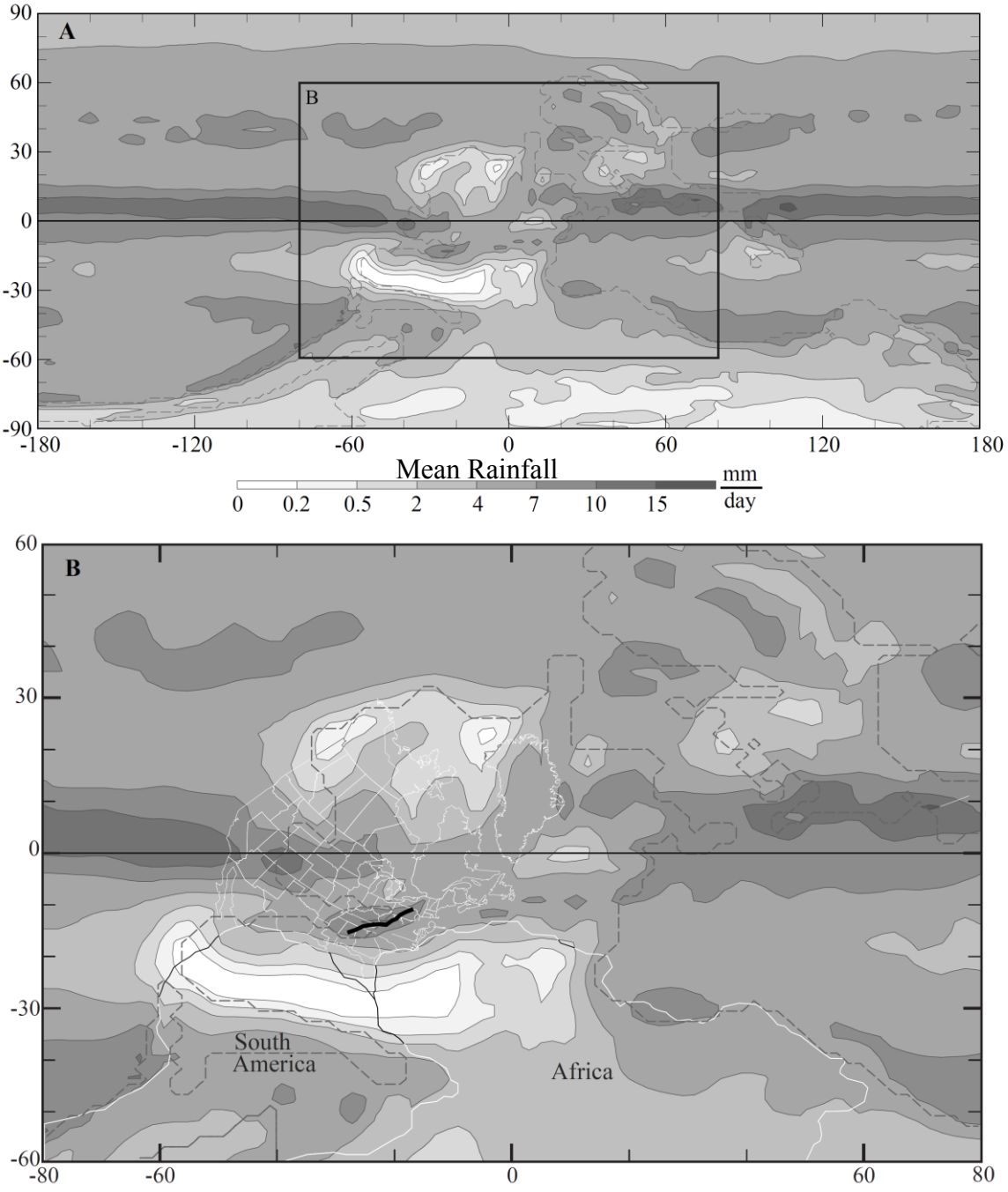
A
B
90
60
30
0
-30
-60
-90
-180
-120
-60
0
60
120
180
Mean Rainfall
0
0.2
0.5
2
4
7
10
15
mm
day
B
60
30
0
-30
-60
-80
-60
0
60
80
South
America
Africa

projection (see Figure 4). Although this projection distorts high latitudes, the developing Appalachian Mountains remain within approximately 40° of the equator and lie largely east-west.

Syntectonic elevation can affect both orographic precipitation and the erosivity of a given amount of precipitation during the formation of an orogenic belt. We have therefore determined the approximate elevation at each cross-section from the estimated elevations (Scotese, in prep.) used as input for the GENESIS 2 GCMs described above. Elevation estimates used in these models are speculative and cannot be independently verified. However, the pattern of elevations mimic modern analogues.

4. RESULTS

4.1. Deformation

Measurements of Alleghenian deformation on 29 cross-sections through the Appalachian foreland show strong variability along-strike in both the amount of total displacement and style of deformation (Figs. 5 and 6). First, the qualitative assessment of thrust sheet displacement shows that thrusting is mostly ramp-on-ramp in the Central Appalachians from the northern end of the Virginia Promontory through the Pennsylvania Embayment (sections 1-12; Figure 5). By contrast, first order thrust sheets in the Southern Appalachians (sects 15 to 29) show more displacement because flat-on-flat ramp relationships are more common. The most displacement appears to have occurred between the Tennessee Embayment and Virginia Promontory (sections 14 to 23) for which approximately 60% of first order thrust sheets are flat-on-flat. However, between sections 24 to 29 flat-on-flat structures drop to ~43% and small displacement ramp-on-ramp structures to ~45% indicating relatively moderate displacement.

Measured deformation values follow similar trends to those for ramp-flat geometry (Fig. 6; Tables 3 and 4). Total displacement, $\mathcal{D}$, reaches a maximum nearest sections 19 to 22 and 14 through the Pine Mountain thrust sheet in the Tennessee Embayment, decreasing north and south along the strike of the mountain belt. To the north, total displacement drops from ~172 km in section 19 to ~112 km in section 18. The total displacement for section 14 is ~169 km south of which it to ~136 km in section

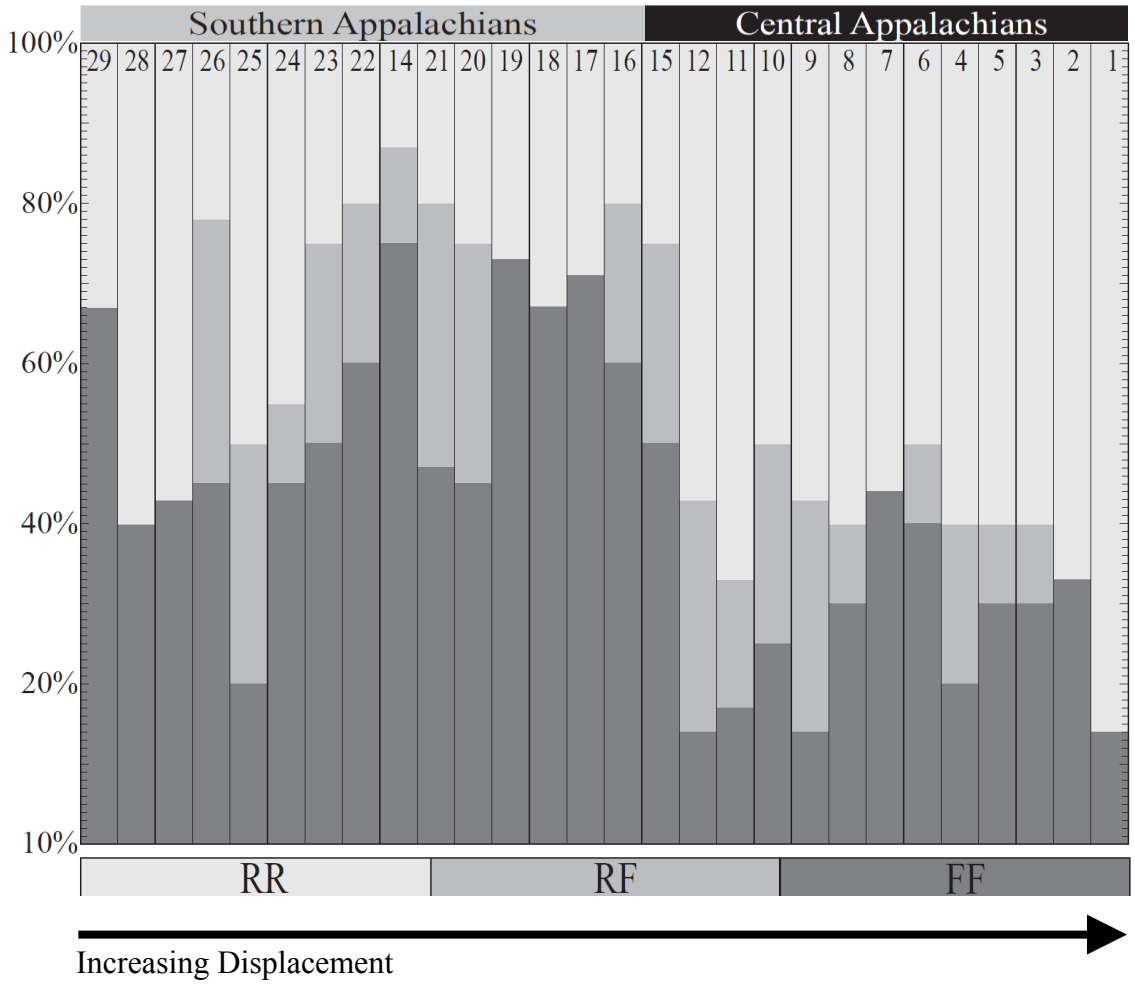

Figure 5: Qualitative assessment of thrust sheet displacement from ramp-flat geometry. The percentage of ramp-on-ramp (RR), ramp-on-flat (RF), and flat-on-flat (FF) thrusts in each section. See Figure 1 for location. RR, RF, and FF structures suggest low, intermediate, and high amounts of thrust sheet displacement respectively (Suppe and Namson, 1979; Suppe, 1983). By this measure, the cross sections may be placed in three groups: 1) RR-dominant (sects **1** to **12**), 2) FF-dominant (sects **15** to **23** and **14**), and 3) RR-FF-dominant (sects **24** to **29**).

23 and ~112 km in section 24. Fault slip decreases to both the northeast and southwest (Fig. 6A, Table 4). Cross-sections 1 to 12 from the Central Appalachians display the least amount of total displacement. $\mathcal{D}$ ranges from ~31 to 80 km, and is on average ~63 km. Sections 27 to 29 in the Southern Appalachians also show relatively low total displacement ranging from ~61.4 to 64.5 km. Sections 15 to 18 and 24 to 26 show moderate total displacement ranging from ~82 to 112 km and averaging ~99 km (Fig. 6A; Table 4). The least average displacement per thrust sheet is in sections 1 to 12 in the Central Appalachians (sections 1 to 12). Between these sections there is little change in average displacement per thrust sheet along-strike. Average thrust sheet displacement increases to the south and in sections 14 to 29 ranges ~8.8-21.1 km. Thrust sheets in the vicinity of the Pine Mountain thrust show extremely variable average displacement ranging from ~9.3 km in section 20 to ~21.1 km in section 14. By contrast, bulk shortening, ΔL, is significantly greater in sections 27 to 29 than in the Central Appalachians (sections 1 to 12). Bulk shortening values generally decrease to the north.

The area of eroded rock material, $\mathcal{E}$, shows a near identical pattern to that of $\mathcal{D}$ along-strike (Fig. 6B). $\mathcal{E}$ is largest nearest the Pine Mountain thrust sheet (sections 20 to 22 and 14). In the Central Appalachians (sections 1 to 12), $\mathcal{E}$ decreases to relatively low values. In the Southern Appalachians in Alabama and Georgia (sections 27 to 29) the area of eroded material also drops to values comparable to that of the Central Appalachians.

Figure 6: Summary plots of deformation in the Appalachian Fold and Thrust Belt. For all plots, the x-axis is the distance along strike measured from the present-day coastal plain onlap of Tertiary sediments. (A) Total displacement, $\mathcal{D}$, per cross-section measured on first order thrust sheets and second order structures plotted on the left vertical axis. Also plotted on the right vertical axis is the bulk percent shortening, ΔL. (B) The total area of eroded rock material, $\mathcal{E}$, plotted on the left vertical axis and average cross-sectional area of thrust sheets, $\bar{A}$, plotted on the right vertical axis. The standard error of length measurements is approximately ± 0.17 km. (C) Average ramp angle measured with respect to local footwall bedding for each cross-section. $\bar{\phi}$ is the average first order ramp angle per section and $\bar{\phi}_t$ is the average second-order ramp angle for each section. Standard error of angle measurements is approximately ± 1.05°. (D) Average total thrust sheet displacement – includes first- and second-order measurements of displacement. See Figure 1 and Table 2 for definition of variables.

Summary plots of deformation in the Appalachian Fold and Thrust Belt

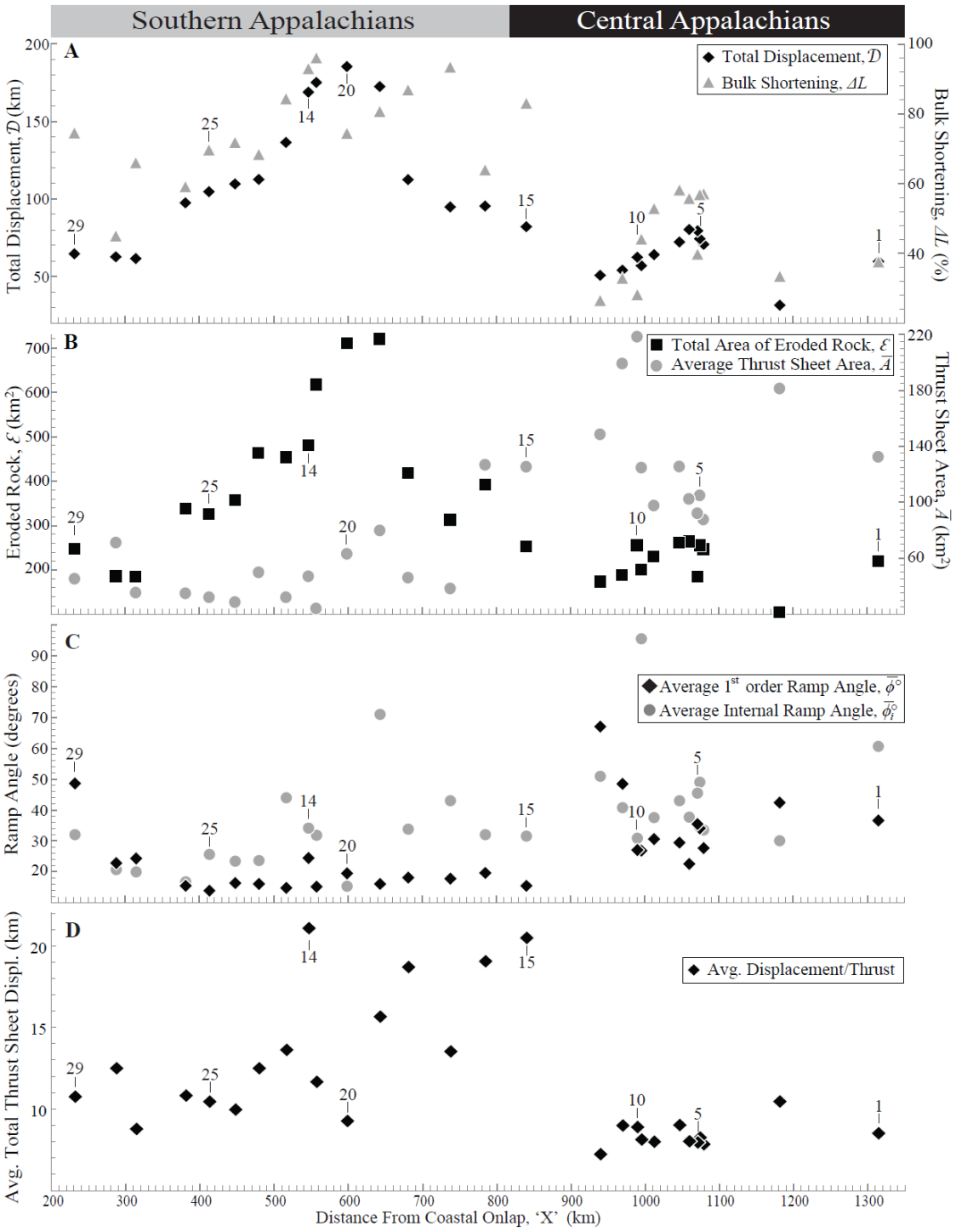
Southern Appalachians
Central Appalachians
A
Total Displacement, $\mathcal{D}$
Bulk Shortening, ΔL
Total Displacement, $\mathcal{D}$ (km)
Bulk Shortening, ΔL (%)
B
Total Area of Eroded Rock, $\mathcal{E}$
Average Thrust Sheet Area, $\bar{A}$
Eroded Rock, $\mathcal{E}$ (km^2)
Thrust Sheet Area, $\bar{A}$ (km^2)
C
Average 1st order Ramp Angle, $\bar{\phi}^\circ$
Average Internal Ramp Angle, $\bar{\phi}_i^\circ$
Ramp Angle (degrees)
D
Avg. Displacement/Thrust
Avg. Total Thrust Sheet Displ. (km)
Distance From Coastal Onlap, 'X' (km)

Table 3.

Averages of Deformation Measurements by Cross Section

sect	X	$\bar{\ell}$	$\bar{t}$	$\bar{T}$	$\bar{h}$	$\bar{h}_\iota$	$\bar{d}$	$\bar{d}_\iota$	$\bar{E}$	$\bar{E}_\iota$	$\bar{\phi}$	$\bar{\phi}_\iota$
#	*km*	*km*	*km*	*km*	*km*	*km*	*km*	*km*	km^2	km^2	*deg*	*deg*
1	1315	22.7	3.6	5.8	4.5	1.9	6.1	8.5	8.5	28.5	9.8	36.6
2	1182	31.3	3.5	5.8	5.1	3.3	4.5	6.0	10.5	20.2	14.9	42.3
3	1079	12.4	3.5	7.1	4.2	3.6	7.6	1.0	7.8	26.6	3.7	27.6
5	1074	13.1	3.0	8.0	3.4	2.3	8.2	0.4	8.2	28.3	0.9	34.0
4	1071	20.0	2.4	4.6	3.7	3.8	6.2	5.7	7.9	17.9	2.6	35.4
6	1060	14.4	3.2	7.1	3.3	2.8	7.9	0.4	8.0	26.1	1.2	22.4
7	1047	15.5	3.2	8.1	4.3	3.0	8.8	0.8	9.0	32.1	2.4	29.4
8	1013	12.1	3.6	8.1	4.4	4.5	8.7	3.2	8.0	31.1	11.9	30.6
9	996	18.5	3.6	6.8	3.3	2.8	7.9	0.8	8.1	28.0	2.2	26.8
10	990	27.6	4.0	7.9	4.0	2.4	6.2	9.3	9.0	27.0	33.3	27.0
11	970	27.4	3.3	7.3	4.1	2.0	8.5	0.9	9.0	31.0	2.1	48.4
12	940	27.3	3.1	5.5	4.6	4.0	6.3	1.2	7.2	22.7	3.7	67.0
15	841	24.7	2.8	5.1	3.4	3.8	20.1	1.8	20.5	61.6	6.7	15.3
16	785	29.9	4.3	4.3	4.4	3.5	17.9	5.6	19.1	74.4	19.8	19.5
17	738	14.5	2.7	2.7	3.8	1.5	12.9	4.4	13.5	43.8	6.4	17.7
18	681	21.6	2.1	2.1	4.2	1.2	18.4	0.9	18.7	69.3	1.2	18.0
19	643	19.4	2.2	4.1	4.0	1.3	15.4	3.1	15.7	65.1	3.9	16.0
20	599	12.5	2.3	5.1	4.0	0.7	8.9	1.9	9.3	35.4	1.5	19.4
21	558	13.0	1.9	1.9	4.2	1.6	10.7	4.6	11.7	42.7	9.4	15.1
14	547	22.7	2.1	2.1	3.0	2.4	18.3	4.4	21.1	54.9	13.8	24.4
22	517	16.2	2.0	2.0	3.7	0.5	12.7	2.4	13.6	45.3	0.7	14.7
23	480	18.3	2.7	2.7	4.1	4.0	11.5	3.1	12.5	46.4	15.4	15.9
24	448	13.9	2.1	2.1	3.6	2.4	9.0	3.7	10.0	30.4	7.6	16.2
25	413	15.0	2.1	2.1	3.6	2.4	9.5	3.1	10.4	34.1	9.6	13.8
26	381	18.3	1.9	1.9	3.6	2.7	9.9	2.7	10.8	34.6	8.9	15.4
27	314	13.3	2.7	2.7	2.9	2.6	7.7	2.4	8.8	23.4	7.1	24.2
28	288	27.8	2.6	2.6	3.0	1.9	9.6	3.6	12.5	29.7	9.3	22.8
29	232	14.4	3.2	3.2	4.2	3.2	10.5	1.3	10.8	48.7	4.1	48.6

Table 4.

Totals of Deformation Measurements by Cross Section

sect	X	d	d_i	$\mathcal{D}$	E	E_i	$\mathcal{E}$	$\bar{A}$	L_0	L_d	ΔL	d
#	km	km	km	km	km^2	km^2	km^2	km^2	km	km	%	km
1	1315	42.5	17.0	59.5	199.6	19.7	219.2	132.5	158.9	99.3	37.5	42.5
2	1182	13.5	17.8	31.4	60.6	44.6	105.2	181.4	94.0	62.6	33.4	13.5
3	1079	68.5	2.0	70.5	239.6	7.3	246.9	87.8	123.7	53.2	57.0	68.5
5	1074	73.8	0.4	74.2	254.3	0.9	255.2	104.9	130.7	56.5	56.8	73.8
4	1071	62.3	17.0	79.3	179.2	5.1	184.3	92.3	199.7	120.4	39.7	62.3
6	1060	79.4	0.8	80.1	261.4	2.4	263.8	102.4	144.0	63.9	55.6	79.4
7	1047	70.4	1.7	72.1	256.5	4.9	261.4	125.7	124.1	52.0	58.1	70.4
8	1013	60.7	3.2	63.9	217.9	11.9	229.7	97.8	121.0	57.2	52.8	60.7
9	996	55.2	1.7	56.9	196.2	4.4	200.5	124.8	129.1	72.3	44.0	55.2
10	990	43.0	18.7	62.2	188.9	66.5	255.4	218.3	221.1	158.9	28.1	43.0
11	970	51.2	2.7	53.9	186.3	2.1	188.4	199.1	164.4	110.5	32.8	51.2
12	940	44.1	6.4	50.6	158.5	14.7	173.2	148.7	190.8	140.3	26.5	44.1
15	841	80.2	1.8	82.0	246.3	6.7	253.0	125.4	98.8	16.9	82.9	80.2
16	785	89.7	5.6	95.3	372.2	19.8	392.0	126.9	149.3	54.0	63.8	89.7
17	738	90.3	4.4	94.7	306.5	6.4	312.9	38.5	101.5	6.8	93.3	90.3
18	681	110.5	1.8	112.3	415.8	2.3	418.1	46.2	129.4	17.2	86.7	110.5
19	643	169.1	3.1	172.2	716.1	3.9	720.0	80.0	213.7	41.5	80.6	169.1
20	599	177.5	7.6	185.1	707.3	3.1	710.4	63.2	249.2	64.0	74.3	177.5
21	558	161.1	13.8	174.9	598.0	18.7	616.7	24.1	182.4	7.5	95.9	161.1
14	547	146.5	22.1	168.6	439.2	41.4	480.6	47.2	181.6	13.0	92.8	146.5
22	517	126.5	9.7	136.2	452.8	0.7	453.5	32.2	161.7	25.6	84.2	126.5
23	480	103.1	9.4	112.4	417.1	46.1	463.3	49.9	164.8	52.3	68.2	103.1
24	448	98.4	11.1	109.5	334.4	22.8	357.1	28.8	152.7	43.3	71.7	98.4
25	413	95.1	9.4	104.5	306.8	19.2	326.0	32.2	150.2	45.8	69.5	95.1
26	381	89.2	8.1	97.3	311.0	26.8	337.8	35.0	164.9	67.6	59.0	89.2
27	314	54.1	7.3	61.4	163.5	21.2	184.6	35.5	93.2	31.8	65.8	54.1
28	288	48.2	14.3	62.5	148.6	37.2	185.8	71.2	139.1	76.6	44.9	48.2
29	232	63.2	1.3	64.5	243.6	4.1	247.8	45.5	86.7	22.2	74.4	63.2

Measured values for average thrust sheet area and ramp angle within both first- and second-order structures generally increase from south to north. Neither of these shows a maximum near the Pine Mountain thrust sheet. In addition, throughout the Central and Southern Appalachians second order ramp angles tend to be greater than those of first-order thrusts (Fig. 6C; Table 3).

$\mathcal{D}$, ΔL, $\mathcal{E}$, $\bar{A}$, and $\overline{D}$ are minimum estimates. In the Southern Appalachians a significant portion of existing thrust sheets have been heavily eroded so that only a fraction of their true dimensions is preserved. Hence, measurements of $\mathcal{D}$, ΔL, $\mathcal{E}$, $\bar{A}$, and $\overline{D}$ likely become further from the true value with increasing exhumation to the south. It is therefore possible, for example, that the total displacement, $\mathcal{D}$, remains constant south of the Virginia Promontory or even increases. In the Central Appalachians erosion of thrust sheets is much lower than to the south. Section 2 is the only cross-section in which all deformation measurements are true values. Oddly, it shows the least total displacement and area of eroded rock (Fig. 6). This may be due to much of the shortening being accommodated by folding.

4.2. Modeled Rainfall

Our purpose is to compare deformation to erosion. Our proxy for erosion is mean annual rainfall. We determined mean annual rainfall for the Carboniferous and Permian Periods from the GENESIS 2 GCM described above.

In the Early Mississippian (~360 Ma) model, mean annual precipitation rates gradually decrease southward (Fig. 7A). The Central Appalachians (sections 1 to 12) at this time received relatively little rainfall (~2.1-3.8 mm/day) in comparison to the Southern Appalachians, but show a steep increase in rate from north to south. Precipitation rate in the Southern Appalachians (sections 14-26) is moderate (~4.2-4.7 mm/day) and increases slightly to the south. Sections 27-29, of northern Alabama and Georgia receive the most intense rainfall compared to sections to the north.

In the Middle Mississippian (~340 Ma), modeled precipitation rate is generally lower than in the Early Mississippian. Rates in the Central Appalachians (sections 1 - 12) become higher than in the Southern Appalachians (sections 14 - 29). Mean annual rainfall in the Central Appalachians increases from ~3.2 mm/day in section 1 to maximum between sections 4 and 8 of ~3.5-3.9 mm/day mean rainfall. To the south, modeled precipitation rate decreases reaching a minimum of ~2.3 -2.5 mm/day in section 29.

In the Mid-Late Mississippian (~300-320 Ma) the average precipitation increases by approximately 5 mm/day. In the Late Mississippian model, peak mean annual rainfall occurs in the vicinity of the Pine Mountain thrust sheet (sections 19 – 14; Figs. 4 and 7A). Average rate of precipitation in the Central Appalachians is lower than the Southern Appalachians reaching a minimum of ~4.8-7.5 mm/day in section 1. In the Late Pennsylvanian (~300 Ma) the average precipitation rate for the Central and Southern Appalachians has dropped back down by ~5 mm/day. The modeled rate is

Figure 7: Summary of results from the GENESIS 2 global climate model. (A) mean annual precipitation results (Grossman et al., 2002) and (B) estimated elevation (Scotese et al., 1999; Scotese, 2002) at 280, 300, 320, 340, and 360 Ma. (A) is a model result but (B) is model input. Models M, were run with higher mountains; m, lower mountains; a, pCO_2 = 280 ppm; b, pCO_2 =1120 ppm. Rainfall and topography for each section is defined by its value at the center-point of that section. The standard error of measurement for mean annual precipitation from the model results is approximately ± 0.08 mm/day. Error in the value *X* through time is a function of model resolution. The error is judged to be within ~3.75° of the plotted position. (C) Base map showing modern geographic location of each cross-section.

Summary of results from the GENESIS 2 global climate model

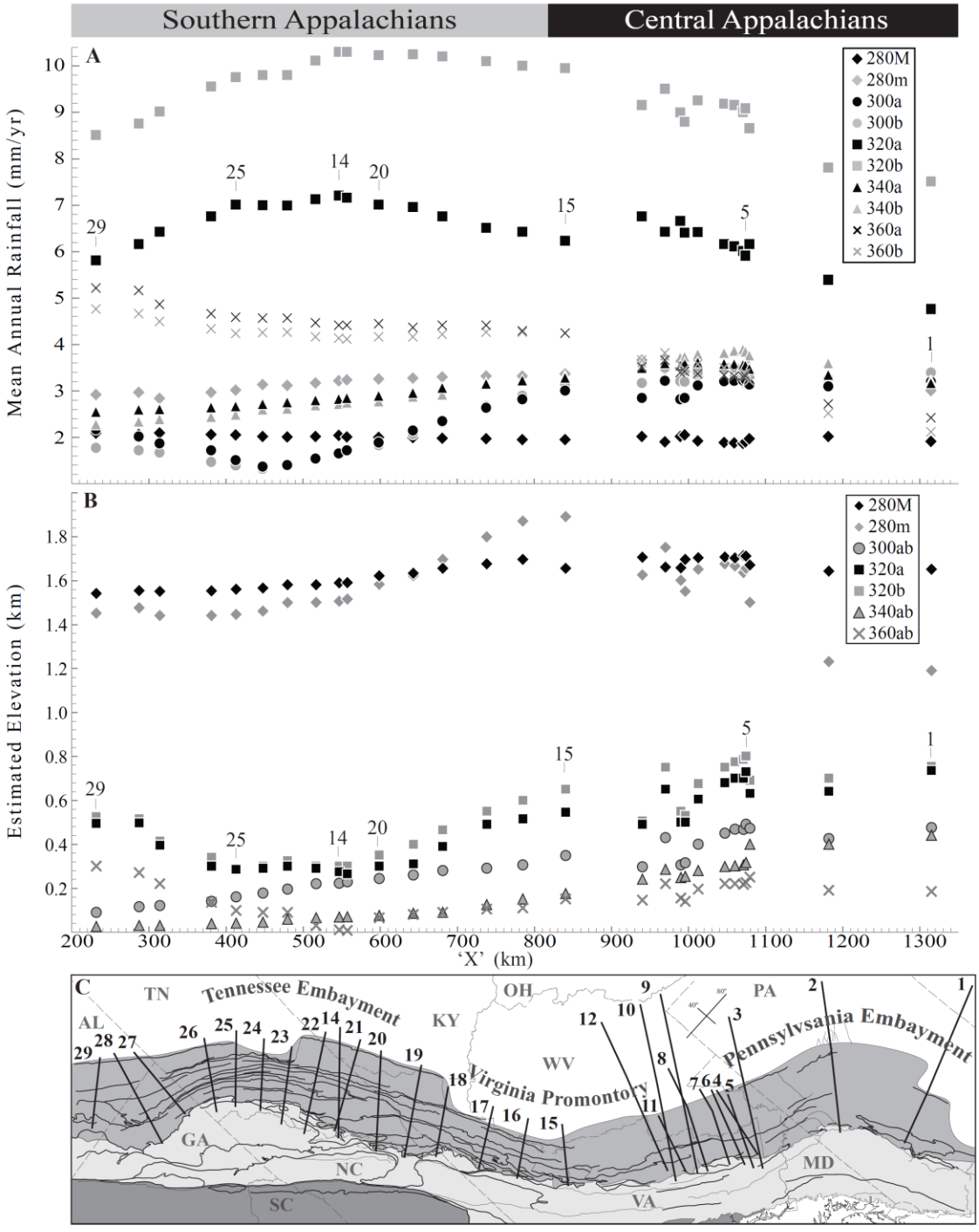
Southern Appalachians
Central Appalachians
A
Mean Annual Rainfall (mm/yr)
280M
280m
300a
300b
320a
320b
340a
340b
360a
360b
B
Estimated Elevation (km)
280M
280m
300ab
320a
320b
340ab
360ab
'X' (km)
C
TN
Tennessee Embayment
AL
KY
OH
PA
WV
Virginia Promontory
Pennsylvsahia Embayment
GA
NC
SC
VA
MD

Figure 8: Total rainfall, P_t, between 280 and 360 Ma. The rate of precipitation that we measure for each cross-section is held constant for the 10 Ma before and following each modeled time period. For example, at 320 Ma the average precipitation rate, *P,* for section 1 is ~7.5 mm/day. We then assume that the precipitation rate is ~7 mm/day, for every day between 310-330 Ma. We consider only the time period between 280 and 360 Ma. Therefore, the measured precipitation rates for the 280 and 360 Ma models are held constant for only 20 m.y. Hence, P_t is approximately equal to the equation shown where T_1 is the start of the time period for which cumulative precipitation will be calculated and T_2 is the end of this period. *P* is the measured value for mean annual precipitation in megameters at each time step and *t* is the number of years for which *P* is held constant.

Total rainfall, P_t, between 280 and 360 Ma

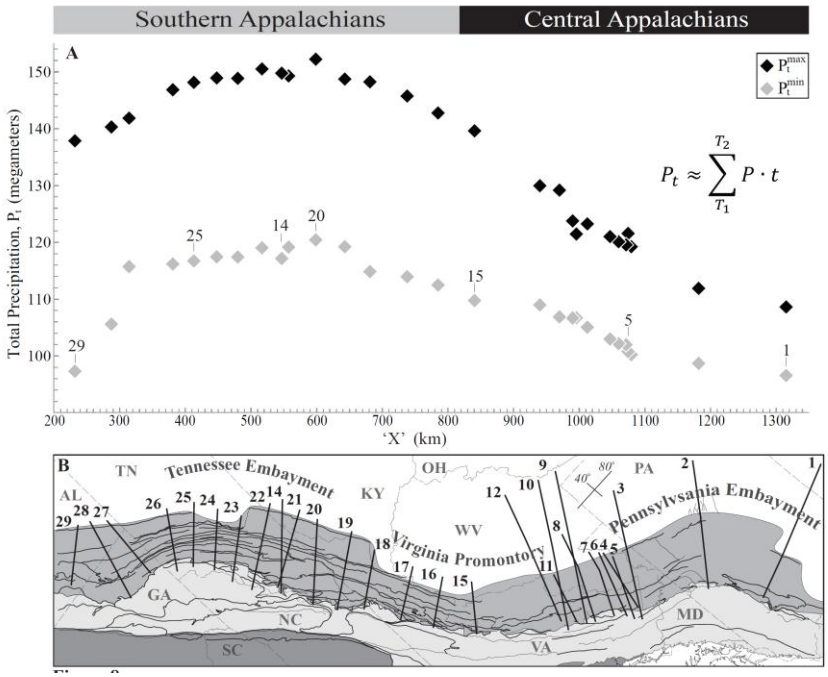
Southern Appalachians
Central Appalachians
A
Total Precipitation, Pt (megameters)
'X' (km)
$P_t \approx \sum_{T_1}^{T_2} P \cdot t$
B
TN
Tennessee Embayment
AL
KY
OH
WV
PA
Pennsylvsania Embayment
Virginia Promontory
GA
NC
SC
VA
MD

again highest in the Central Appalachians (~2.8-5.6 mm/day) and decreases to a minimum of ~1.3-1.4 mm/day in section 24 (Fig. 7A). South of section 24, rates pick back up increasing southward. In the Artinskian Stage of the Cisuralian Epoch (~280 Ma) model 'c' predicts the highest rate of precipitation at the southern end of the Central Appalachians (sections 8-12), decreasing to the north and south. The lowest rate of mean annual rainfall for model 'c' is predicted in sections 27-29. By contrast, model 280d predicts the highest rainfall intensity in the southern-most sections decreasing to the north. Model 280d uses a revised topography with lower mountains which may explain the inversion of trends along-strike. Nevertheless, we can make the general statement that there is little change in the rate of precipitation between the Late Pennsylvanian and late Permian. Additionally, at 280 Ma, the rate of precipitation is fairly consistent along-strike.

Total rainfall accumulation, P_t, received during the formation of the Appalachian Fold and Thrust belt (Figure 8) shows focused precipitation between sections 18 and 26, near the Pine Mountain Fault where $\mathcal{D}$, $\mathcal{E}$, and ΔL are also highest. To the south (sections 27-29) rainfall decreases only slightly while to the north there is a much more drastic decrease in total rainfall between sections 12 and 3. Sections 1 and 2 near the Pennsylvania Embayment (sections 1 and 2) receive the least rainfall at this time and show relatively little change between them.

5. DISCUSSION

5.1. Assumptions

This research is based on the 29 cross-sections from Woodward (1985) and GENESIS 2 GCM of global mean annual precipitation. We assume that the rainfall amount is a valid proxy for amount of erosion.

The erosive effectiveness of a given amount of rainfall may change with bedrock strength, temperature, vegetation, storm frequency, and seasonality among others (Langbein and Schumm, 1958; Schumm, 1968; Jansen and Painter, 1974; Jiongxin, 2005; Assouline and Ben-Hur, 2006). Increased bedrock strength will lower the erosive power of precipitation. Hence, a region with higher bedrock strength would require more rainfall to achieve a certain amount of erosion than a region with lower bedrock strength (Hack, 1973). Temperature controls the loss of water by evapotranspiration (Langbein and Schumm, 1958). Increased temperature will decrease soil moisture leaving less groundwater available for runoff. Therefore, more precipitation is required for a given amount of erosion produced by runoff in a warmer climate than in a cool climate (e.g., Langbein and Schumm, 1958). Plant biomass or vegetative cover can affect erosion in several ways (e.g., Garner, 1959; Williams et al., 1996; Favis-Mortlock and Guerra, 1999). For example, increased production rates for various arborescent plants such as trees and conifers will increase soil surface canopy cover. This effectively shields the earth's surface from the impact of raindrops thereby reducing the erosivity of a given

amount of rainfall (Jiongxin, 2005; Nearing et al., 2005). In addition, rooting of these plants in the soil allows greater retention of water which also retards erosion (Berner and Holdren, 1979). The density of vegetation, in turn, is principally controlled by rainfall (Garner, 1959). In general, more rainfall will enhance plant production and increase vegetative cover. However, annual periods of low precipitation will cause some types of vegetation to disappear. Consequently, high seasonality that includes annual hot drought periods, followed by monsoonal rains will lead to more erosion than would be expected from the annual amount of rain alone (Wilson, 1973).

The vegetation during the Carboniferous Allegheny orogeny primarily included conifers and their close relatives, the cordaiteans, early seed plants known as seed ferns, and plants that reproduce with spores (ferns, lycopsids, and sphenophytes) (Mapes and Gastaldo, 1986). Relatively little is known of the soil forming and holding ability of Paleozoic plants, because ground covering plants growing at high altitudes and in sub-humid environments have a sparse fossil record (Algeo and Scheckler paper). Among modern plants, perennial grasses, which radiated in the Neogene, have best ability to hold soil. In the absence of grasses, soil erosion at high altitudes and in sub-humid environments was probably faster during the Carboniferous than it is today. Envisioning a typical montane landscape, Carboniferous alpine wetlands and meadows could have been inhabited by lycopsids, sphenopsids and ferns, many of which may have had rhizomes (modified stems that grow along the ground giving rise to numerous upright stems), allowing them to carpet the land surface. However, the rooting depth of these plants and the plants themselves remain unknown. Thus, montane wetlands and

meadows may have eroded more quickly in the Carboniferous than at present, due to the absence of perennial grasses. In terms of their ability to withstand erosion, the montane forests of the Carboniferous, which were presumably inhabited by early conifers and cordaitean trees with a fern, lycopsid and sphenopsid understory, may have been similar to modern montane forests in their resistance to erosion.

5.2. Deformation, Rainfall, and Erosion

Our results show that erosion during the Allegheny orogeny was higher in the Southern Appalachians than in the North. The average area of eroded material produced in each section in the Southern Appalachians is ~404 km^2. In addition, deformation in the vicinity of the Pine Mountain thrust sheet (sections 19 to 24 and 14) is significantly higher than the immediate surrounding area. For example, total displacement in section 19 is ~1.5 times greater than section 18, which is ~39 km away. The total displacement for section 14 is ~1.5 times greater than in section 23, which is ~66 km away. By contrast, deformation was lowest in Central Appalachians. Sections 1 to 12 have on average ~63 km of total displacement with ~ 44% bulk shortening. The average area of eroded material produced in each section in the Central Appalachians is ~215 km^2. Precipitation data from the GENESIS 2 GCM indicate relatively high cumulative rainfall for sections 19 to 24 and 14, ranging from ~$148x10^3$ to $152x10^3$ km (see Figure 8). Cumulative rainfall in the Central Appalachians is ~$108x10^3$ to $130x10^3$ km. Following both early speculation (Hoffman and Grotzinger, 1993) and model results (e.g., Persson

et al., 2004) increased rainfall causes rapid erosion reducing both the normal stress and shear resistance on active frictional faults. This would promote increased displacement on faults. Likewise, a lack of rainfall reduces erosion leading to more overburden on faults. The increased normal stress due to burial will, in turn, increase shear resistance on frictional faults. The net result of reduced erosion is to inhibit motion on faults.

Bedrock strength may also affect the efficiency of erosion in the Appalachians, as has been suggested for active mountain belts such as Taiwan (Li, 1976; Liu, 1982; Liew et al., 1993; Fuller et al., 2003). Specifically, change in lithology northeast of section 19 may explain the jump in deformation. Mississippian red beds and Pennsylvanian conglomerates, sandstones, shales, and coals increase in thickness north of section 18 (Thomas, 1989 in Hatcher et al., 1989). Southwest of section 18 the stratigraphy is dominated by Upper Mississippian mudstones and sandstones, and laterally discontinuous units of Pennsylvanian conglomerates, sandstone, mudstone, and coal (Thomas, 1989 in Hatcher et al., 1989). However, southwest of the Pine Mountain thrust, between sections 14 and 23, no such change in lithology has been observed. Therefore, erosion removed more material south of section 24, perhaps due to differences in exposed lithologies at the time of active deformation.

Estimates of elevation from Scotese (per. comm., 2010) may have enhanced precipitation west of peak elevation through much of Appalachian development (see Fig. 7). During this time, the area around the Pine Mountain thrust sheet is interpreted to occupy a regional low in elevation (Fig. 7B on page 35; Scotese in prep.). Only the 300 Ma precipitation model predicts less rainfall in this region than in surrounding areas. The

trend of increased deformation and precipitation near slope break is similar to what has been observed in the Himalayas. Specifically, in the Himalayas, the youngest AFT cooling ages are confined to a region with focused orographic precipitation (Bookhagen et al., 2005), steep longitudinal river profiles (Seeber and Gornitz, 1983), high relief and rapid exhumation (Thiede et al., 2004).

The synthesis of erosion and deformation in the Appalachian fold and thrust belt presented here suggests that the Southern Appalachians experienced more rainfall during the Carboniferous Allegheny orogeny. In addition, thrusts are displaced further during this time. We therefore conclude that a correlation between rainfall as a proxy for erosion and fault displacement exists in the case of the Appalachian fold and thrust belt.

6. CONCLUSIONS

We have compared modeled rainfall to measured thrust sheet displacement, geometry, and intensity of internal deformation in the Appalachian fold and thrust belt. What make the Appalachians interesting is that during the Carboniferous Allegheny orogeny the orogen experienced changing climatic conditions. Mean annual precipitation determined from GENESIS 2 Global Climate Model simulations (Grossman, per. comm.) varied from tropical to arid conditions as the collision both moved north and grew in breadth and height. Our main conclusions:

1) The Southern Appalachians, which receive more net rainfall than other regions, generally show more displacement, deeper exhumation, and shallower ramp angles than regions to the north.
2) Ramp angles gradually increase from ~20° in the south to ~50° in the north.
3) The average thrust sheet area generally increases from south to north.
4) The vicinity of the Pine Mountain thrust in the Southern Appalachians experienced the most displacement (~1.5 times that of the Central Appalachians) and bulk shortening (~1.6 times the Central Appalachians) and produced the most eroded material (~1.5 times the Central Appalachians). The Pine Mountain thrust sheet region received ~20% more net rainfall during the time interval from 360 to 280 Ma than did the Central Appalachians.

REFERENCES

Assouline, S., Ben-Hur, M., 2006. Effects of rainfall intensity and slope gradient on the dynamics of interrill erosion during soil surface sealing. Catena (Giessen) 66, 211-220.

Barron, E.J., 1995. Warmer worlds; global change lessons from Earth history. World Survey of Climatology 16, 71-94.

Berner, R.A., Holdren, G.R., Jr., 1979. Mechanism of feldspar weathering; II, Observations of feldspars from soils. Geochimica et Cosmochimica Acta 43, 1173-1186.

Bonan, G.B., Pollard, D., Thompson, S.L., 1992. Effects of horeal forest vegetation on global climate. Nature 359, 716-716.

Bookhagen, B., Thiede, R.C., Strecker, M.R., 2005. Abnormal monsoon years and their control on erosion and sediment flux in the high, arid Northwest Himalaya. Earth and Planetary Science Letters 231, 131-146.

Cobbold, P.R., Davy, P., Gapais, D., Rossello, E.A., Sadybakasov, E., Thomas, J.C., Tondji Biyo, J.J., de Urreiztieta, M., 1993. Sedimentary basins and crustal thickening. Sedimentary Geology 86, 77-89.

Crowley, T.J., Yip, K.J.J., Baum, S.K., 1993. Milankovitch cycles and Carboniferous climate. Geophysical Research Letters 20, 1175-1178.

Dadson, S.J., Hovius, N., Chen, H., Dade, W.B., Hsieh, M.-L., Willett, S.D., Hu, J.-C., Horng, M.-J., Chen, M.-C., Stark, C.P., Lague, D., Lin, J.-C., 2003. Links between

erosion, runoff variability and seismicity in the Taiwan Orogen. Nature (London) 426, 648-651.

Dallmeyer, R.D., Wright, J.E., Secor, D.T., Jr., Snoke, A.W., 1986. Character of the Alleghanian Orogeny in the Southern Appalachians; Part II, Geochronological constraints on the tectonothermal evolution of the eastern Piedmont in South Carolina. Geological Society of America Bulletin 97, 1329-1344.

Favis-Mortlock, D.T., Guerra, A.J.T., 1999. The implications of general circulation model estimates of rainfall for future erosion; a case study from Brazil. Catena (Giessen) 37, 329-454.

Garner, H.F., 1959. Stratigraphic-sedimentary significance of contemporary climate and relief in four regions of the Andes mountains. Geological Society of America Bulletin 70, 1327-1368.

Grossman, E.L., Pollard, D., Scotese, C.R., Hyde, W.T., 2002. Oxygen isotope and global climate model (GCM) investigations of Permo-Carboniferous climate. Abstracts with Programs - Geological Society of America 34, 501.

Hack, J.T., 1973. Stream-profile analysis and stream-gradient index. Journal of Research of the U. S. Geological Survey 1, 421-429.

Hatcher, R.D., Jr., Thomas, W.A., Geiser, P.A., Snoke, A.W., Mosher, S., Wiltschko, D.V., 1989. Alleghanian Orogen. In: Hatcher, R.D., Jr., Thomas, W.A., Viele, G.W. (Eds.), The Appalachian-Ouachita Orogen in the United States. Geological Society of America, Boulder, Colorado, pp. 233-318.

Hoffman, P.F., Grotzinger, J.P., 1993. Orographic precipitation, erosional unloading, and tectonic style. Geology (Boulder) 21, 195-198.

Hoffman, P.F., Tirrul, R., King, J.E., St-Onge, M.R., Lucas, S.B., 1988. Axial projections and modes of crustal thickening, eastern Wopmay Orogen, Northwest Canadian Shield. Special Paper - Geological Society of America 218, 1-29.

Jackson, M.J., 1988. Lower Proterozoic Cowles Lake foredeep reef, N.W.T., Canada. Memoir - Canadian Society of Petroleum Geologists 13, 64-71.

Jansen, J.M.L., Painter, R.B., 1974. Predicting sediment yield from climate and topography. Journal of Hydrology 21, 371-380.

Keith, A., 1895. New structural features in the Appalachians. Science 1, 58.

Langbein, W. B. and Schumm, S. A.,1958. Yield of sediment in relation to mean annual precipitation. Transactions American Geophysical Union 39, 1076-1084.

Leturmy, P., Mugnier, J.L., Vinour, P., Baby, P., Colletta, B., Chabron, E., 2000. Piggyback basin development above a thin-skinned thrust belt with two detachment levels as a function of interactions between tectonic and superficial mass transfer; the case of the Subandean Zone (Bolivia). Tectonophysics 320, 45-67.

Li, Y.H., 1976. Denudation of Taiwan Island since the Pliocene Epoch. Geology (Boulder) 4, 105-107.

Liew, P.M., Pirazzoli, P.A., Hsieh, M.L., Arnold, M., Barusseau, J.P., Fontugne, M., Giresse, P., 1993. Holocene tectonic uplift deduced from elevated shorelines, eastern Coastal Range of Taiwan. Tectonophysics 222, 55-68.

Liu, T.-K., 1982. Tectonic implication of fission track ages from Central Range, Taiwan. Proceedings of the Geological Society of China 25, 22-37.

Merle, O., Abidi, N., 1995. Approche expérimentale du fonctionnement des rampes émergentes. Bulletin de la Société géologique de France 166, 439-450.

Mitra, G., Boyer, S.E., 1986. Energy balance and deformation mechanisms of duplexes. Journal of Structural Geology 8, 291-304.

Mugnier, J.L., Baby, P., Colletta, B., Vinour, P., Bale, P., Leturmy, P., 1997. Thrust geometry controlled by erosion and sedimentation; a view from analogue models. Geology (Boulder) 25, 427-430.

Nearing, M.A., Jetten, V., Baffaut, C., Cerdan, O., Couturier, A., Hernandez, M., Le Bissonnais, Y., Nichols, M.H., Nunes, J.P., Renschler, C.S., Souchere, V., van Oost, K., 2005. Modeling response of soil erosion and runoff to changes in precipitation and cover. Catena (Giessen) 61, 131-154.

Otto-Bliesner, B.L., 1993. Tropical mountains and coal formation: a climate model study of the Westphalian (306 Ma). Geophysical Research Letters 20, 1947-1950.

Persson, K.S., Garcia-Castellanos, D., Sokoutis, D., 2004. River transport effects on compressional belts; first results from an integrated analogue-numerical model. Journal of Geophysical Research 109, B01409, doi: 10.1029/2002JB002274.

Persson, K.S., Sokoutis, D., 2002. Analogue models of orogenic wedges controlled by erosion. Tectonophysics 356, 323-336.

Pollard, D., Schulz, M., 1994. A model for the potential locations of Triassic evaporite basins driven by paleoclimatic GCM simulations. Global and Planetary Change 9, 233-249.

Pollard, D., Thompson, S.L., 1994. Computational aspects of the GENESIS earth systems modeling project. In: Ames, W.F. (Ed.), 14th International Association for Mathematics and Computers in Simulation (IMACS) World Congress on Computation and Applied Mathematics, Atlanta, Georgia.

Pollard, D., Thompson, S.L., 1995. Use of a land-surface-transfer scheme (LSX) in a global climate model (GENESIS): The response to doubling stomatal resistance. Global and Planetary Change 10, 129-161.

Pollard, D.D., Thompson, S.L., 1997. Climate and ice-sheet mass balance at the last glacial maximum from the genesis version 2 global climate model. Quaternary Science Reviews 16, 841-863.

Price, P.H., 1931. The Appalachian structural front. Journal of Geology 39, 24-44.

Rodgers, J., 1970. The tectonics of the Appalachians. Wiley-Interscience, New York, New York, United States.

Roe, G.H., Montgomery, D.R., Hallet, B., 2003. Orographic precipitation and the relief of mountain ranges. Journal of Geophysical Research 108.

Rogers, H.D., 1850. On the structural features of the Appalachians. American Association for the Advancement of Science, Proceedings, 113-115.

Rogers, H.D., Rogers, W.B., 1843. On the physical structure of the Appalachian Chain, as exemplifying the laws which have regulated the elevation of great mountain chains generally. American Journal of Science and Arts 44, 359-362.

Schumm, S.A., 1968. Speculations concerning paleohydrologic controls of terrestrial sedimentation. Geological Society of America Bulletin 79, 1573-1588.

Scotese, Boucot, A.J., and McKerrow, W.S., 1999. Gondwanan paleogeography and paleoclimatology, Journal of African Earth Scinces, v. 28, no. 1., pp. 99-114.

Secor, D.T., Jr., Snoke, A.W., Bramlett, K.W., Costello, O.P., Kimbrell, O.P., 1986. Character of the Alleghanian Orogeny in the Southern Appalachians; Part I, Alleghanian deformation in the eastern Piedmont of South Carolina. Geological Society of America Bulletin 97, 1319-1328.

Seeber, L., Gornitz, V., 1983. River profiles along the Himalayan Arc as indicators of active tectonics. Tectonophysics 92, 335-367.

Shaler, N.S., 1877. On the existence of the Alleghany division of the Appalachian Range within the Hudson Valley. The American Naturalist, 627-628.

Sloan, L.C., Rea, D.K., 1996. Atmospheric carbon dioxide and early Eocene climate; a general circulation modeling sensitivity study. Palaeogeography, Palaeoclimatology, Palaeoecology 119, 275-292.

St-Onge, M.R., 1984. The muscovite-melt bathograd and low-P isograd suites in north-central Wopmay Orogen, Northwest Territories, Canada. Journal of Metamorphic Geology 2, 315-326.

Suppe, J., 1983. Geometry and kinematics of fault-bend folding. American Journal of Science 283, 684-721.

Suppe, J., Namson, J., 1979. Fault-bend origin of frontal folds of the western Taiwan fold-and-thrust belt. Petroleum Geology of Taiwan, 1-18.

Thiede, R.C., Bookhagen, B., Arrowsmith, J.R., Sobel, E.R., Strecker, M.R., 2004. Climatic control on rapid exhumation along the Southern Himalayan Front. Earth and Planetary Science Letters 222, 791-806.

Thomas, W. A., 1991. The Appalachian-Ouachita rifted margin of southeastern North America. Geological Society of America Bulletin 103, 415-431.

Thompson, P.H., 1989. An empirical model for metamorphic evolution of the Archaean Slave Province and adjacent Thelon tectonic zone, north-western Canadian Shield. Geological Society Special Publications 43, 245-263.

Whipple, K.X., 2009. The influence of climate on the tectonic evolution of mountain belts. Nature Geoscience 2, 97-104.

Whipple, K.X., Meade, B., 2002. Erosional control of orogenesis; approximate analytical solution for a two-sided, frictional orogenic wedge at steady state. Eos, Transactions, American Geophysical Union 83, F1323-F1324.

Williams, J., Nearing, M., Nicks, A., Skidmore, E., Valentin, C., King, K., Savabi, R., 1996. Using soil erosion models for global change studies. Journal of Soil and Water Conservation 51, 381-385.

Willis, B., 1893. Part 2; The mechanics of Appalachian structure. United States Geological Survey Annual Report 13, Part 2, 211-281.

Wilson, K.M., Pollard, D., Hay, W.W., Thompson, S.L., Wold, C.N., 1994. General circulation model simulations of Triassic climates; preliminary results. Special Paper - Geological Society of America 288, 91-116.

Wilson, L., 1973. Variations in mean annual sediment yield as a function of mean annual precipitation. American Journal of Science 273, 335-349.

Woodward, N.B., 1985. Valley and Ridge thrust belt; balanced structural sections, Pennsylvania to Alabama. University of Tennessee, Department of Geological Sciences, Knoxville, Tennessee.

VITA

Name: Sean Kristian Steen

Address: Department of Geology and Geophysics
Texas A&M University
MS 3115 TAMU
College Station, TX 77845

Email Address: seanksteen@tamu.edu

Education: B.S., Geology, Texas A&M University at College Station, 2008
M.S., Geology, Texas A&M University at College Station, 2011